Journal of Fluids and Structures (2002) **16**(8), 1177–1191
doi:10.1006/jfls.2002.0463 available online at http://www.idealibrary.com on IDEAL®

A NONLINEAR FLUID–STRUCTURE INTERACTION ANALYSIS OF A NEAR-BED SUBMARINE PIPELINE IN A CURRENT

K. Y. Lam, Q. X. Wang and Z. Zong

Institute of High Performance Computing, 89-C Science Park Drive, 02-11/12 The Rutherford Singapore Science Park I, 118261, Singapore

(Received 14 November 2000; and in final form 13 November 2001)

A negative lift force (attraction) can be induced on a near-bed pipeline in a horizontal current due to asymmetric flow. This negative lift force has a significant influence on the behaviour of the near-bed pipeline, causing two remarkable failure patterns. One failure pattern is due to stability loss, and the pipeline fully rests on the seabed. The other is due to the excessive stress or deformation even if the pipeline is stable in a position between the original equilibrium position and the seabed. A quantitative method to assess these two failure patterns by combining boundary element and finite element methods is proposed in this paper. This is a nonlinear fluid–structure interaction problem, and an iteration procedure is used herein to solve it. Numerical examples reveal that there exists a critical current velocity, above which the pipeline fails. The relationship between the critical velocity and the distance from the pipeline to the seabed is given.

1. INTRODUCTION

Several environmental forces, among which are waves and currents (lift, drag, scour), seafloor soil movements (mudslides, earthquakes, sand wave migration), and accidental loadings (impact, underwater explosion), have significant influences on the behaviour of submarine pipelines near the seabed. These forces might induce excessive stresses in pipes in unfavorable cases, causing pipeline failures. As a complicated fluid–structure interaction problem, the behaviour of submarine pipelines subjected to various loads has been extensively studied both theoretically and experimentally. Fredsøe & Hansen (1987), Magda (1997) and Sarpkaya & Isaacson (1981) presented forces on submarine pipelines in steady flows and in waves, respectively. The hydrodynamic forces on submarine pipelines in waves/currents have been investigated by Neill & Hinwood (1998), Damgaard & Whitehouse (1999), and Sabag *et al.* (2000). Chiew (1990), Grass & Hosseinzadeh-Dalir (1995), and Cevik & Yüksel (1999) discussed the scour depth under pipelines. In addition, Bijker (1990) studied the pipeline-sand wave interaction. Takahashi & Bando (1998) and Kershenbaum *et al.* (2000) presented the behaviour of marine structures under seismic faults. The response of free-span pipelines to impact was studied by Chung & Cheng (1996), and the response of submarine pipelines to underwater explosion was studied by Zong & Lam (2000*a*).

In this paper, a supported submarine pipeline with a small gap between the original equilibrium position and the seabed is studied. When a submarine pipeline in a horizontally steady current is far away from the seabed, it is not influenced by the seabed

0889-9746/02/081177 + 15 $35.00/0

and experiences a zero net force in the vertical direction due to the symmetry of the flow. However, when the pipeline is near the seabed, the presence of the seabed changes the symmetric flow scenario, by assigning a higher velocity to the flow between the pipeline and the seabed and a lower velocity to the flow above the pipeline. When the gap between the pipeline and the seabed is very narrow, a very high flow velocity is expected from the continuity equation. From Bernoulli's equation, the pressure in the gap between the pipeline and the seabed is very low, and the pressure of the flow above the pipeline is high, resulting in a downward force (Milne-Thomson 1968; Zdravkovich 1985; Kalghatgi & Sayer 1997) on the pipeline (see Figure 1).

Some early experimental investigations (Bagnold 1974; Bearman & Zdravkovich 1978; Sarpkaya & Isaacson 1981) have been performed to evaluate forces on cylinders some distance away from the seabed. From the turbulent spectra, it is concluded that the vortex shedding does not take place at the downstream of the pipe at small gap ratios. This means that the flow around the pipeline very near the seabed can be considered as a steady problem. In addition, Grass *et al.* (1984) investigated effects of the bed proximity and velocity gradients in the approaching bed boundary layer. They found that small gap effects were much complicated by the presence of any boundary layer in the approaching bed shear flows. Fredsøe & Hansen (1987) investigated effects of shear in the incoming flow, and Reynolds number. They found that shear in the incoming flow could influence the lift force, and the effect of the Reynolds number was much smaller on the lift force, because an evenly distributed wake pressure does not contribute to the lift force. This conclusion was also reached by Aschenbach (1969). Moreover, viscosity is restricted to a thin boundary layer, and effects of viscosity are smaller on the vertical force. Hence, in this paper, we restrict ourselves to the vertical force, which results from the imbalance between the pressures on the top of and below the pipeline. The fluid is here assumed to be ideal, and effects of the boundary layer and the approaching bed shear flows are neglected.

Potential flow theory is used in this paper. Therefore, when a gap exists, the downward force acting on the pipeline is in fact the same as the lift force, but in the opposite direction (negative lift force). The attracting force of the seabed tends to pull a submarine pipeline down to the seabed, exerting high bending stresses in the pipeline. This fluid–structure interaction problem is nonlinear, and is studied in this paper. Our investigations have revealed that the negative lift force is so large that it is likely that the submarine pipeline could fail even in normal operational environments. When potential flow theory is used, the analytical solution for the lift force is available (Müller 1929; Grass *et al.* 1995), and the formulation of the complex potential is obtained as a summation of an infinite series. In this paper, two numerical methods, the boundary element method (BEM) and the finite

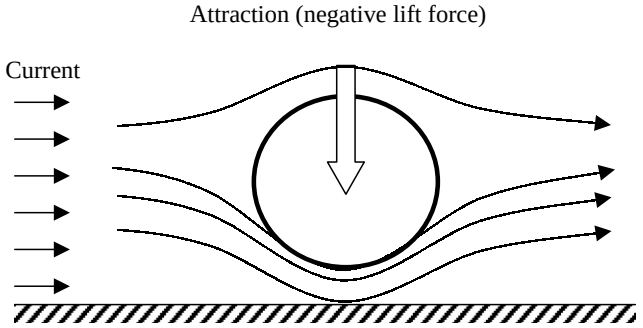

Figure 1. The negative lift for a submarine pipeline in a current.

element method (FEM), are also investigated and used to obtain the negative lift force on a pipeline. FEM is used to discretize the pipeline response equation. By equating the fluid force to the bending force, we obtain a nonlinear fluid–structure interaction equation governing the near-bed pipeline motion in a current. An iterative scheme is used, and two failure modes (instability failure and strength failure) are discussed. Numerical examples show that a bifurcation occurs between different failure modes. This means that there exists a critical current velocity, above which a near-bed pipeline will become unstable and finally fully rest on the seabed. Below the critical velocity, the near-bed pipeline, even in the stable state, may also fail due to high bending stresses. The relationship between the critical velocity and the gap between the pipeline and the seabed is given. Finally, useful information for the pipeline design and operation is provided.

2. CURRENT FORCE ON SUBMARINE PIPELINES IN SEMI-INFINITE WATER

2.1. Governing Equation

Consider a circular steel pipe covered with a layer of reinforced concrete. The coordinate system is shown in Figure 2(a) with the x-axis coincident with the undeformed pipeline axis, the y-axis pointing outward horizontally, and the z-axis in the deflection direction. Suppose that the pipeline is in a steady current. The current velocity is U_0, and the distance between the central line of the undeformed pipeline and the seabed is D_0. Suppose the pipe length L is much greater than the pipe outer radius R_c, i.e., $L \gg R_c$, then the pipe can be simplified as an Euler beam fixed at both ends, and its deflection is described by $w(x)$. From the above definition, we have $D(x) = D_0 - w(x)$, and assume that $w(x)$ is small relative to the pipe length L.

In this paper, the fluid is assumed irrotational and incompressible, and thus there exists a potential $\phi(x, y, z)$ due to the presence of the pipe, satisfying

$$\frac{\partial^2 \phi}{\partial x^2} + \frac{\partial^2 \phi}{\partial y^2} + \frac{\partial^2 \phi}{\partial z^2} = 0 \tag{1}$$

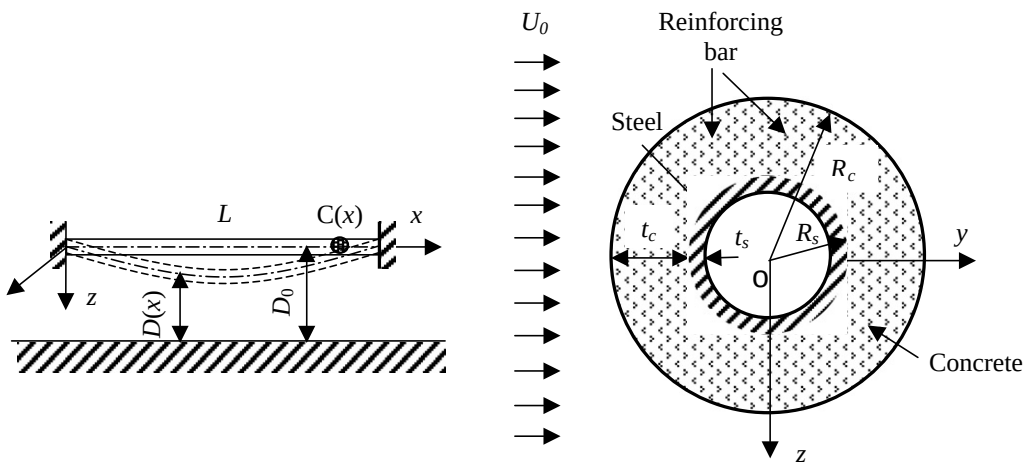

(a) The coordinate system (b) The pipe section C(x)

Figure 2. A submarine pipeline in a current.

throughout the fluid domain, with boundary conditions

$$\frac{\partial \phi}{\partial y} = U_0 \quad \text{at } \sqrt{x^2 + y^2 + z^2} \to \infty, \tag{2}$$

$$\frac{\partial \phi}{\partial n} = 0 \quad \text{on the pipe surface,} \tag{3}$$

where $n = (n_x, n_y, n_z)$ denotes the three-dimensional unit vector normal to the pipe surface.

A lot of computational effort is needed to solve the above equations due to the nature of the three-dimensional flow. However, the computation can be greatly simplified by using the slenderness assumption (Newman 1978) defined by the following relations:

$$\varepsilon = R_c/L \ll 1, \quad n_x = O(\varepsilon), \quad n_y = O(1), \quad n_z = O(1). \tag{4}$$

On this basis, near the body, we have

$$\frac{\partial \phi}{\partial x} \ll \left(\frac{\partial \phi}{\partial y}, \frac{\partial \phi}{\partial z}\right), \quad \frac{\partial^2 \phi}{\partial x^2} \ll \left(\frac{\partial^2 \phi}{\partial y^2}, \frac{\partial^2 \phi}{\partial z^2}\right). \tag{5}$$

Thus, Laplace's equation is reduced to a two-dimensional form

$$\frac{\partial^2 \Phi}{\partial y^2} + \frac{\partial^2 \Phi}{\partial z^2} = 0, \tag{6}$$

where Φ replaces the three-dimensional potential,

$$\Phi = \phi(y, z; x). \tag{7}$$

Here the dependence on x is included to emphasize that this potential will vary slowly along the length of the structure, as a result of the change in the lateral deformation. Boundary conditions (2) and (3) can then be replaced by

$$\frac{\partial \Phi}{\partial y} = U_0 \quad \text{at } \sqrt{y^2 + z^2} \to \infty, \tag{8}$$

$$\frac{\partial \Phi}{\partial N} = 0 \quad \text{on the pipe surface.} \tag{9}$$

Here $N = (N_y, N_z)$ denotes the two-dimensional unit vector normal to the pipe surface in the y–z plane. The potential Φ corresponds to the solution of the two-dimensional flow problem at each section along the pipe length, and thus is easily found.

2.2. Current-Induced Fluid Force

Based on the assumptions above, the potential flow around a cylinder placed near a wall can be readily found (Müller 1929). The analytical solution to equations (6), (8) and (9), in terms of a complex potential $\omega = \omega(s)$, is given by

$$\omega = \sum_{j=0}^{\infty} \left(\frac{m_j}{s - S_j} + \frac{m_j}{s - \bar{S}_j}\right), \tag{10}$$

where s is the complex coordinate

$$s = y + \mathrm{i}z, \tag{11}$$

and

$$m_0 = U_0 R_c^2, \quad m_{j+1} = m_j \frac{R_c^2}{(2D_0 - Y_j)^2}, \tag{12}$$

$$Y_0 = D_0, \quad Y_{j+1} = D_0 - \frac{R_c^2}{2(2D_0 - Y_j)}, \tag{13}$$

$$S_j = \mathrm{i} Y_j, \quad \bar{S}_j = -\mathrm{i} Y_j. \tag{14}$$

The complex potential, (equation (10), describes the flow with a farfield velocity U_0 around a cylinder with a radius R_c, and the centerline of the cylinder is located at the distance D_0 away from the seabed. Using this complex potential, we can obtain the negative lift force.

The boundary value problem defined by equations (6)–(9) can also be effectively solved using the boundary element method (BEM). In the BEM formulation, the semi-infinite fluid domain is approximated by a rectangular domain Ω (size $20R \times 20R$) as shown in Figure 3. Define $\Gamma = \partial\Omega$, and the boundary of Ω is composed of the boundaries of the water domain under consideration, the pipe surface and the seabed. Then the boundary conditions can be rewritten as

$$\frac{\partial \Phi}{\partial N} = -U_0 \quad \text{on the inflow boundary,}$$

$$\frac{\partial \Phi}{\partial N} = U_0 \quad \text{on the outflow boundary,}$$

$$\frac{\partial \Phi}{\partial N} = 0 \quad \text{on the pipe surface,} \tag{15}$$

$$\frac{\partial \Phi}{\partial N} = 0 \quad \text{on the seabed and the upper boundary of the fluid domain.}$$

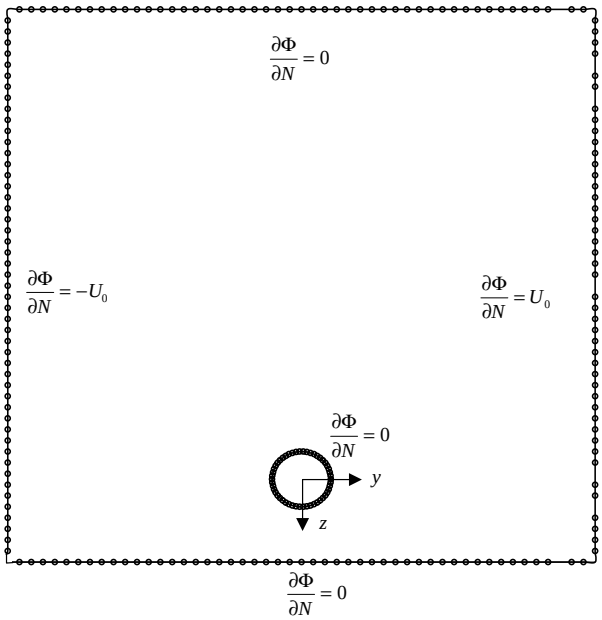

Figure 3. The BEM mesh and boundary conditions.

The boundary is discretized into m constant boundary elements. The potential Φ can be easily solved using BEM (Brebbia 1978). From Bernoulli's equation, the flow pressure p on the pipe surface can be obtained, and then we get the fluid force f induced by the current.

The following dimensionless coefficients are defined:

$$c = \frac{2f}{\rho A U_0^2}, \quad d = \frac{D(x) - R_c}{2R_c}, \tag{16, 17}$$

where A is the cross-section area of the pipe. The results obtained from the analytical solution [equation (10)] and BEM are shown in Figure 4. For comparison, FEM is also used to obtain the fluid force. The FEM mesh is shown in Figure 5. The FEM results are also shown in Figure 4. From this figure, we conclude that both the BEM and FEM results and the exact solution obtained from equation (10) are in very good agreement.

2.3. Rational Approximation of Fluid Force

Although there exists an analytical solution of equation (10), it converges slowly. Therefore, for computational efficiency, a rational approximation of the fluid force is developed based on the BEM results.

From Figure 4, we see that the resultant force coefficient c on a pipe section is only a function of d. To save computational cost in the analysis of fluid–structure interaction later, we may express the relationship between c and d through an explicit equation. Suppose the relation between them can be approximated by the following rational function:

$$c(d) = \frac{A_1 d^2 + A_2 d + A_3}{A_4 d^3 + A_5 d^2 + A_6 d}. \tag{18}$$

There are two reasons for using the above form. One is that c is inversely dependent on d from the numerical results (see Figure 4). To meet this requirement the denominator (a third-order polynomial) is one order higher than the numerator (a second-order polynomial). The other reason is that polynomials are simple, so both denominator and numerator are assumed polynomials.

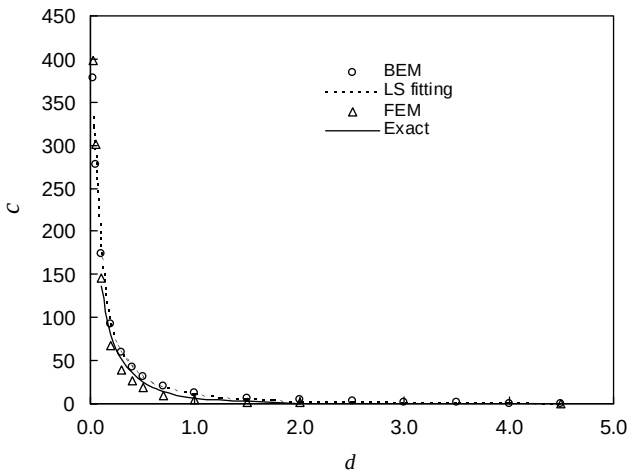

Figure 4. The nondimensional force on the pipe: ○, BEM; ..., LS fitting; △, FEM; —, exact.

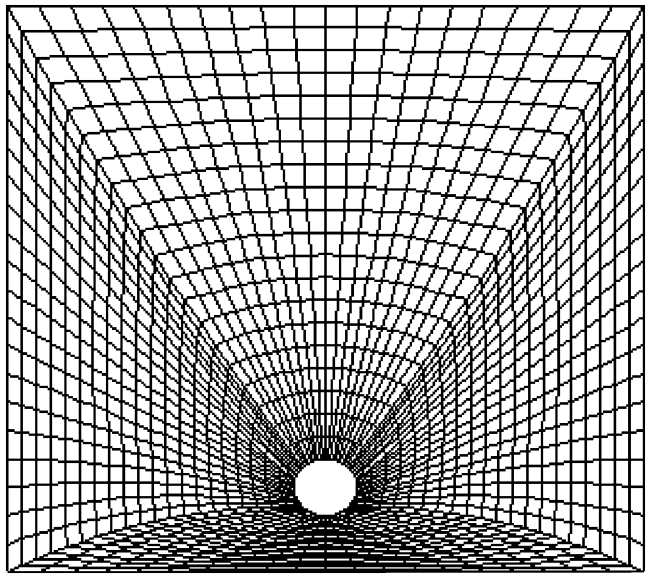

Figure 5. The FEM mesh.

To obtain coefficients $A_1, \ldots, A_6$, we define the following norm as an error indicator:

$$e(A_1, A_2, A_3, A_4, A_5, A_6) = \sum_{i=1}^{n} \left[c(d_i) - c^i_{\mathrm{BEM}}\right]^2, \tag{19}$$

where $c(d_i)$ and c^i_{BEM} are calculated from equations (18) and (16), respectively. This is an unconstrained minimization problem. The standard polytope optimization method (Nelder & Mead 1965) is used to find the minimum of the function $e(A_1, \ldots, A_6)$ of six variables. The optimization results of A_1–A_6 are listed in Table 1.

In this paper, a higher-order form of d and c is also tried. It is found that there is not a great difference between the higher-order form and the form presented above. The results of this approximate fit are shown in Figure 4, where they are also compared with the exact solution (Müller 1929), and the BEM and FEM results. We see that these results are in very good agreement. Using this fitting curve, forces for every iteration step can easily be obtained.

3. THE NONLINEAR RESPONSE OF THE PIPE

3.1. Pipe Modelling

Since the pipe length $L \ll R_c$ and $D_0 \ll L$, the pipe is then simplified as an Euler beam fixed at both ends. Using the coordinate system in Figure 2(a), the response of the pipe is given by

$$EI\frac{\mathrm{d}^4 w(x)}{\mathrm{d}x^4} = f(x), \quad 0 \le x \le L, \quad w(x) \le D_0, \tag{20}$$

where $w(x)$ is the deflection of the pipe. The equivalent bending stiffness EI is defined by

$$EI = E_c I_c + E_s I_s, \tag{21}$$

where $E_c I_c$ and $E_s I_s$ are stiffnesses of concrete and steel, respectively.

TABLE 1
The optimization results

A_1	A_2	A_3	A_4	A_5	A_6	*Error* (e)
2·2327510	12·5462900	0·0243700	0·7668064	0·4358999	0·0236994	0·46777

From equation (16) and the fitting result, we obtain the fluid force $f(x)$,

$$f(x) = \tfrac{1}{2}\rho A U_0^2 c(d), \tag{22}$$

where

$$d = \frac{D(x) - R_c}{2R_c} = \frac{D_0 - w(x) - R_c}{2R_c}.$$

The force $f(x)$ is a non-linear function of the deflection $w(x)$. Therefore, the pipe deflection equation (20) is nonlinear.

In order to solve equation (20), the pipe is discretized using equal length elements. Using Hermite cubic interpolation functions (Reddy 1993), the FEM equation of the pipe is

$$\begin{bmatrix} A & B \\ B^{\mathrm{T}} & C \end{bmatrix} \begin{Bmatrix} W \\ \Theta \end{Bmatrix} = \begin{Bmatrix} F \\ M \end{Bmatrix}, \quad WD_0, \tag{23}$$

where W, $\dot{E}$, F and M are the displacement vector, the bending rotation vector, the external force vector and the moment vector, respectively. F is determined from equation (22), and M is the corresponding equivalent moment. The elements of the sub-matrices A, B and C, which depend on the elastic beam characteristics, are defined as

$$a_{i,\,i-1} = -6\alpha_{i-1}, \quad a_{i,\,i} = 6(\alpha_{i-1} + 6\alpha_i), \quad a_{i,\,i+1} = -6\alpha_i,$$

$$b_{i,\,i-1} = -3\alpha_{i-1}l, \quad b_{i,\,i} = -3\alpha_{i-1}l + 3\alpha_i l, \quad b_{i,\,i+1} = 3\alpha_i l,$$

$$c_{i,\,i-1} = \alpha_{i-1}l^2, \quad c_{i,\,i} = 2\alpha_{i-1}l^2 + 2\alpha_i l^2, \quad c_{i,\,i+1} = \alpha_i l^2,$$

where $\alpha_i = 2EI/l^3$, α_0 and α_n are defined to be zero, and l is the element length.

The response of the pipe can be obtained by solving nonlinear equation (23). Then, according to material mechanics, the cross-section maximum stresses are given by

$$(S_s)_{\max} = E_s R_s \frac{\mathrm{d}^2 w(x)}{\mathrm{d}x^2} = E_s R_s \left(w_1 \frac{\mathrm{d}^2 H_1}{\mathrm{d}x^2} + \theta_1 \frac{\mathrm{d}^2 H_2}{\mathrm{d}x^2} + w_2 \frac{\mathrm{d}^2 H_3}{\mathrm{d}x^2} + \theta_2 \frac{\mathrm{d}^2 H_4}{\mathrm{d}x^2} \right), \tag{24}$$

$$(S_c)_{\max} = E_c R_c \frac{\mathrm{d}^2 w(x)}{\mathrm{d}x^2} = E_c R_c \left(w_1 \frac{\mathrm{d}^2 H_1}{\mathrm{d}x^2} + \theta_1 \frac{\mathrm{d}^2 H_2}{\mathrm{d}x^2} + w_2 \frac{\mathrm{d}^2 H_3}{\mathrm{d}x^2} + \theta_2 \frac{\mathrm{d}^2 H_4}{\mathrm{d}x^2} \right),$$

where $(S_s)_{\max}$ and $(S_c)_{\max}$, E_s and E_c, and R_s and R_c are the maximum stresses, elastic moduli, and the radii of the steel and concrete pipes, respectively. The second-order

derivatives of Hermite cubic interpolation functions are:

$$\frac{\mathrm{d}^2H_1}{\mathrm{d}x^2} = -\frac{6}{l^2}\Big(1 - 2\frac{x - x_e}{l}\Big), \quad \frac{\mathrm{d}^2H_2}{\mathrm{d}x^2} = -\frac{2}{l}\Big(2 - 3\frac{x - x_e}{l}\Big),$$

$$\frac{\mathrm{d}^2H_3}{\mathrm{d}x^2} = -\frac{\mathrm{d}^2H_1}{\mathrm{d}x^2}, \quad \frac{\mathrm{d}^2H_4}{\mathrm{d}x^2} = -\frac{2}{l}\Big(1 - 3\frac{x - x_e}{l}\Big)$$

where x_e is the coordinate value of the left node of the element.

3.2. Solution of the Nonlinear Equation Using Iterative Method

Because equation (23) is nonlinear, it cannot be solved directly. An iterative scheme is used to obtain the solution. The following iterative formula is used:

$$\begin{Bmatrix} W^{n+1} \\ \Theta^{n+1} \end{Bmatrix} = \begin{bmatrix} A & B \\ B^{\mathrm{T}} & C \end{bmatrix}^{-1} \begin{Bmatrix} F(W^n, \Theta^n) \\ M(W^n, \Theta^n) \end{Bmatrix}, \tag{25}$$

where superscript n and $n+1$ denote the nth and $(n+1)$th iterative steps, respectively.

A complete pipe response simulation requires the establishment of static initial conditions, namely the equilibrium configuration due to static loads on the pipe. At the first step, the pipe is in its undeformed orientation, and the distributed force is uniform, so we can easily get the nodal equivalent forces, and then the deflection of the first step, W^1. However, when the pipe has a small deflection, the distributed force on the pipe will not be uniform but a function of W. The equivalent nodal forces are difficult to obtain directly. Therefore, Gauss quadrature (Reddy 1993) is used to get the nodal equivalent forces.

The iteration stops when

$$\sqrt{\sum_{j=1}^{n} (w_j^{i+1} - w_j^i)^2}\varepsilon, \tag{26}$$

where n is the number of nodes used in FEM, w_j^i andw_j^{i+1} are the deflection results of the ith and $(i+1)$th iteration steps, respectively. ε is a specified accuracy tolerance. In this paper, we take $\varepsilon = 10^{-6}$.

The flowchart of the solution of the nonlinear fluid–structure interaction problem is given in Table 2.

3.3. Failure Analysis

The term on the right-hand side of equation (23) is a nonlinear function of the deflection, which has a significant influence on the behaviour of a near-bed pipeline. It becomes very large as the gap between the pipeline and the seabed is very small, and approaches zero if the gap is very large (see Figure 4). Hence, the pipeline is always attracted to the seabed. One of nonlinear effects due to the seabed attraction is that the pipeline suddenly loses its stability and sticks to the seabed, once the current velocity exceeds a critical velocity or once the gap between the pipeline and the seabed is too small. Except for the two ends, the entire pipeline tends to stick to the seabed. This causes excessively high stresses at both ends. The two-dimensional assumption used in this paper will predict infinitely large stresses at both ends. Therefore, the stability loss due to high current velocities or small gaps causes so high stress levels at both ends that they exceed allowable stresses, resulting in pipeline failure. This failure pattern is purely due to stability loss, and thus it is an instability failure pattern.

TABLE 2

The flowchart of solution of the nonlinear fluid–structure interaction problem

1.	Determine the stiffness matrix in equation (23)
2.	Give nodal displacement W^n, nodal rotation Θ^n, nodal force F^n and nodal moment M^n
3.	Obtain nodal F^{n+1} and nodal moment M^{n+1} from equation (22) and Gauss quadrature
4.	Obtain nodal displacement W^{n+1} and nodal rotation Θ^{n+1} from equation (25)
5.	If $\sqrt{\sum_{j=1}^{n}(w_j^{i+1}-w_j^i)^2}\varepsilon$, go to 7
6.	Go to 2
7.	If $W^{n+1}=D_0-R_c$, then unstable
	If $W^{n+1}<D_0-R_c$, end.

TABLE 3

Deflections of the pipe at different current velocities ($D_0=2R_c$)

U_0 (m/s)	$W_{L/2}$(m)	No. of iteration steps
1·0	0·0020	4
3·0	0·0151	6
5·0	0·0435	9
7·0	0·0949	13
9·0	0·2111	37
9·2	0·2372	61
9·2944	0·2821	905
9·2945	0·5000	Unstable

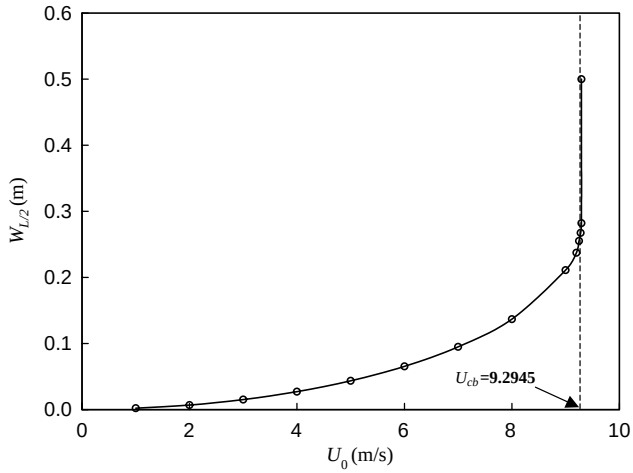

Figure 6. The deflection of the mid-span of the pipe ($D_0=2R_c$) as a function of U_0.

If the current velocity is below the critical velocity, the pipeline under consideration deforms in such a way that it finally stabilises at a position between the seabed and the original equilibrium position. In this case, the strength analysis is the same as that without considering the seabed. The strength failure occurs if the maximum stress $(S_s)_{\max}$ in steel

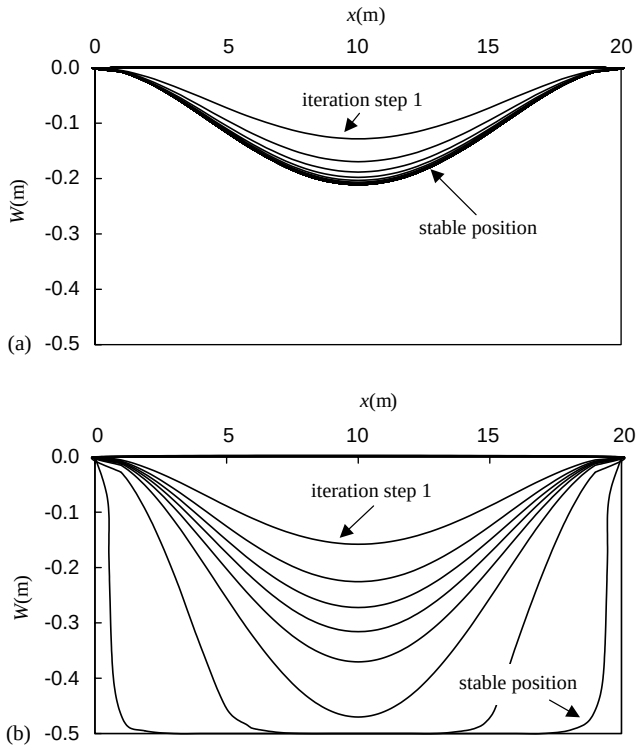

Figure 7. (a) The deflection of the pipe at successive iteration steps ($U_0 = 9{\cdot}0$m/s). (b) The deflection of the pipe at successive iteration steps ($U_0 = 10{\cdot}0$m/s).

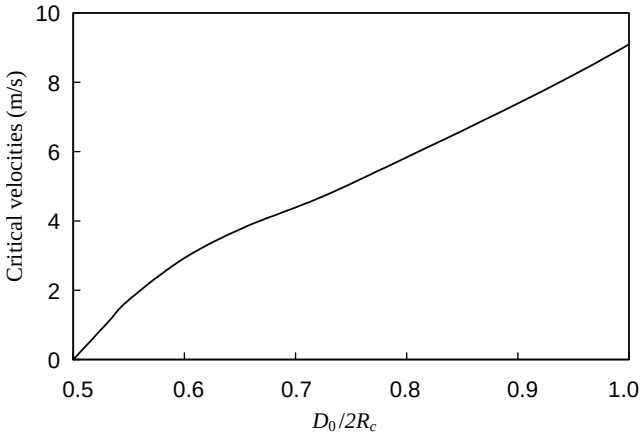

Figure 8. The critical velocities U_{cb} of the instability failure.

exceeds its yielding stress Y_s (i.e., $S_s \geqslant Y_s$), or the maximum stress $(S_c)_{\max}$ in concrete exceeds its yielding stress Y_c (i.e., $S_s \geqslant Y_c$), or the maximum deflection $W_{\max}$ of the pipe exceeds its allowable deflection Y_w.

Therefore, there are two failure patterns. One is the instability failure due to the stability loss under high current velocities or small gaps. The other is the strength failure, which

includes yielding failure and deflection failure, due to high stresses or large deflections even when the pipeline is still stable.

4. RESULTS AND ANALYSIS

Consider the following example: $L = 20\,m$, $E_s = 2{\cdot}11 \times 10^{11}\,\mathrm{N/m^2}$, $\mathrm{R}_s = 0{\cdot}4\,\mathrm{m}$, $t_s = 0{\cdot}012\,\mathrm{m}$ (steel pipe thickness), $E_c = 2.5 \times 10^{10}\,\mathrm{N/m^2}$, $R_c = 0{\cdot}5\,\mathrm{m}$, $\rho_s = 7800\,\mathrm{kg/m^3}$ (steel density), $\rho_c = 2400\,\mathrm{kg/m^3}$ (concrete density), $D_0 = 2R_c$. The pipe is discretized using 20 equal length elements. The nominal values for the strength parameters are as follows: $Y_s = 2{\cdot}5 \times 10^8\,\mathrm{N/m^2}$, $Y_c = 2{\cdot}5 \times 10^7\,\mathrm{N/m^2}$, and $Y_w = 0{\cdot}004$, $L = 0{\cdot}08\,\mathrm{m}$.

First, we use the iteration scheme [equation (25)] to obtain the relation between the current velocities U_0 and the mid-span deflections $W_{L/2}$. The values of the mid-span deflection at different current velocities are given in Table 3 and Figure 6. As the current velocity increases, the mid-span deflection also increases until the point where $U_{cb} = 9{\cdot}2945\,\mathrm{m/s}$. Below this velocity, the iteration scheme [equation (25)] converges to a stable position between the seabed and the original position as shown in Figure 7(a). Above this velocity, the entire pipeline, except for a small portion near both ends, sticks to the seabed as shown in Figure 7(b).

It is clear from the above discussion that the critical velocity U_{cb} depends on the gap between the pipeline and the seabed. Such a relation is obtained by repeatedly using equation (25) for different values of D_0, and is plotted in Figure 8. Physically, a small gap between the pipeline and the seabed will induce a high force on the pipeline as seen from equation (18) or Figure 4. The required current velocity to push the pipeline to stick to the seabed is then low. This relationship is shown in Figure 8, where U_{cb} is a monotonically increasing function of D_0.

In the above, only the instability failure mode was discussed. We now turn to the discussion of the strength failure mode. The stress distributions in the pipe are obtained utilizing equation (24). The stress results for $U_0 = 5.0\,\mathrm{m/s}$ are plotted in Figure 9. As expected, the maximum stresses are found at both ends of the pipe. The maximum stresses of steel and concrete pipes at different current velocities, U_0, with $D_0 = 2R_c$, are shown in Figure 10. From this figure, it is seen that the stresses of both steel and concrete pipes increase monotonically with the current velocity. When the velocity increases to a specific value, the maximum stress equals the yielding stress. This value, shown in Figure 10, is the

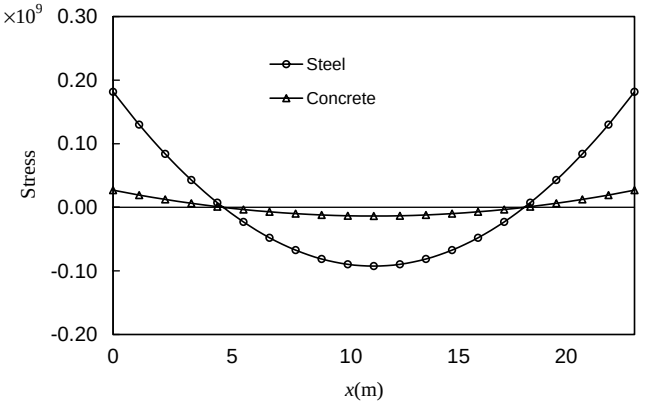

Figure 9. The stress distributions along the pipe ($U_0 = 5{\cdot}0\mathrm{m/s}$).

critical value for the strength failure. The critical velocity for the strength failure of the steel pipe is defined as U_{cys} [Figure 10(a)] and the critical velocity for the strength failure of the concrete pipe is defined as U_{cyc} [Figure 10(b)]. Meanwhile, the maximum deflection is also an increasing function of the current velocity. Once the current velocity is above the critical value, denoted by U_{cw} [Figure 10(c)], the pipeline also fails due to the overdeformation.

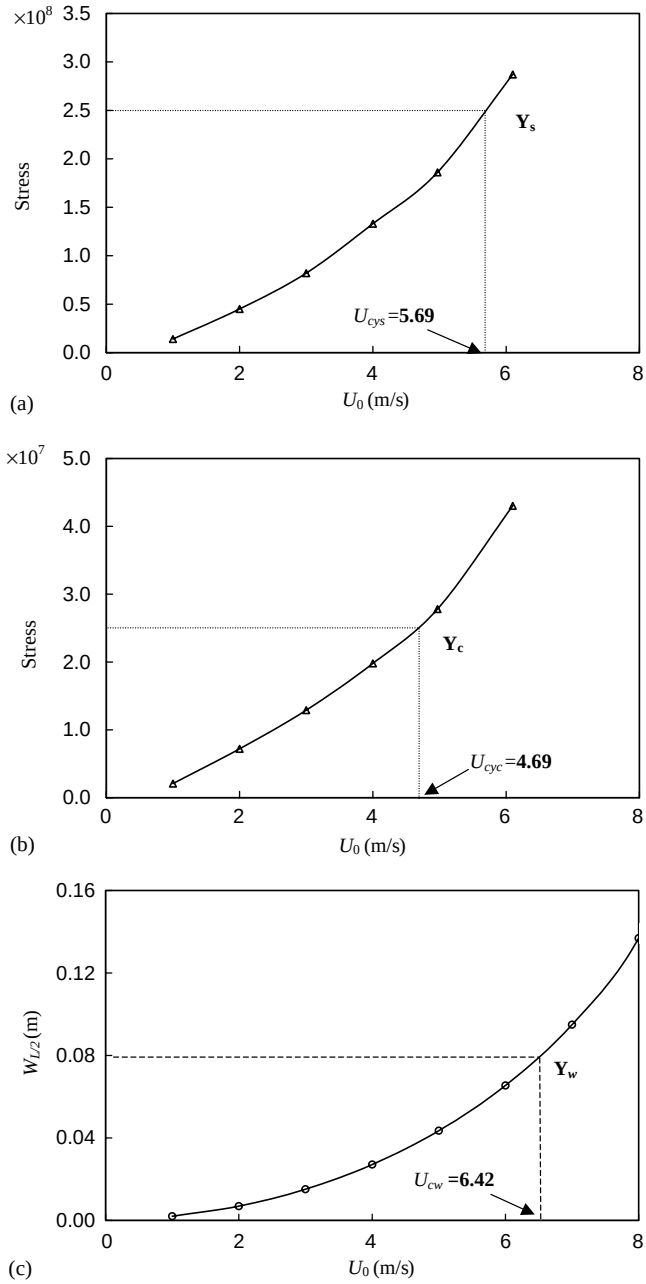

Figure 10. The maximum stress (a) in the steel pipe ($D_0 = 2R_c$), and (b) in the concrete layer of the pipe ($D_0 = 2R_c$). (c) The maximum deflection of the pipe ($D_0 = 2R_c$).

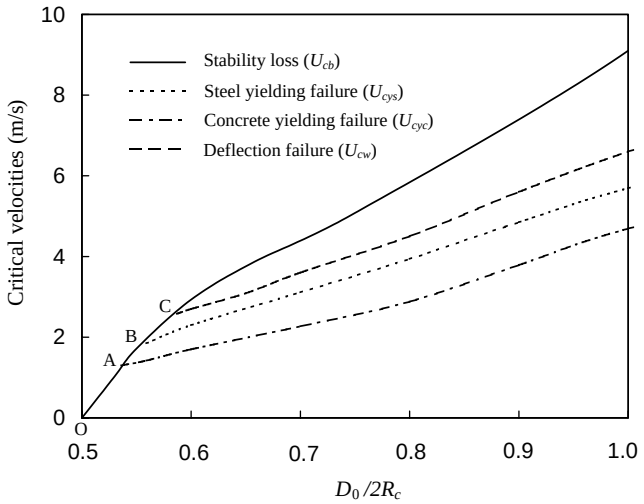

Figure 11. The critical velocities U_{cb}, U_{cys}, U_{cyc} and U_{cw}: —, stability loss (U_{cb}); - - - -, steel yielding failure (U_{cys}); — – —, concrete yielding failure (U_{cyc}); – – –, deflection failure (U_{cw}).

In the above, four critical current velocities are defined to describe four failures. The influence of D_0 on the four critical velocities (U_{cb}, U_{cys}, U_{cyc}, U_{cw}) is plotted in Figure 11. The most interesting feature in the figure is the existence of bifurcation at points A, B and C. From point O to point A on the curve, the instability failure mode dominates strength failure modes. Point A is a bifurcation point, beyond which the concrete pipe fails before the pipeline loses stability, and the instability failure mode will no longer occur from point A.

It should be noted that in our analysis the fluid force becomes infinite when $D_0 \to 0$. This is because the two-dimensional inviscid simplification is used. If a three-dimensional model is used for the fluid domain, the force will be finite when $D_0 \to 0$ (Zong & Lam 2000*b*). The two-dimensional model overestimates the loading on the pipe. In addition, conditions of different failure modes are obtained in this paper without considering their interactions. The interactions between the different failure modes will be studied in our future work.

5. CONCLUSIONS

A nonlinear fluid–structure interaction analysis is proposed in this paper to assess the behaviour of near-bed submarine pipelines in a horizontal steady current. From the studies in this paper, it is concluded that

(i) the seabed has a significant influence on the behaviour of near-bed pipelines in a current. There exist two failure modes: stability loss and strength failure;

(ii) there exists a critical current velocity beyond which pipelines fail either in the mode of stability loss or in the mode of strength failure; and

(iii) when the gap is small, the stability loss dominates the strength failure. As the gap increases, the occurrence of strength failure becomes more likely than stability loss.

The effects of three dimensionality and viscosity will be considered in our future work.

REFERENCES

ASCHENBACH, E. 1969 Distribution of local pressure and skin friction around a circle cylinder I cross-flow up to $Re = 5 \times 10^6$. *Journal of Fluid Mechanics* **34,** 625–639.

Bagnold, R. A. 1974 Fluid forces on a body in shear-flow; experimental use of 'stationary' flow. *Proceedings of the Royal Society London, Series A* **340,** 147–171.

Bearman, P. W. & Zdravkovich, M. M. 1978 Flow around a circular cylinder near a plane boundary. *Journal of Fluid Mechanics* **89,** 33–47.

Bijker, R. J., Van Foeken, A. H., Van der pal, D. S. & Staub, C. A. 1990 Pipeline-sand wave interaction. *Proceedings Pipeline Technology Conference*, pp. 12.13–12.19.

Brebbia C. A. 1978 *The Boundary Element Method for Engineers*. London: Pentench Press.

Cevik, E. & Yüksel, Y. 1999 Scour under submarine pipelines in waves in shoaling conditions. › *ASCE Journal of Waterway, Port, Coastal and Ocean Engineering* **125,** 9–19.

Chiew, Y. M. 1990 Mechanics of local scour around submarine pipelines. *ASCE Journal of Hydrodynamics Engineering*, **116,** 515–529.

Chung, J. S. & Cheng, B.-R. 1996 Nonlinear coupled responses to impact loads on free-span pipeline: torsional coupling, load steps and boundary conditions. *International Journal of Offshore and Polar Engineering* **6,** 53–61.

Damgaard, J. S. & Whitehouse, R. J. S. 1999 Evaluation of marine pipeline on-bottom stability. Part I: hydrodynamics aspects. *Pipeline and Gas Journal* **226,** XXX–XXX.

Fredsøe, J. & Hansen, E. A. 1987 Lift forces on pipelines in steady flow. *ASCE Journal of Waterway, Port, Coastal and Ocean Engineering Division* **113,** 139–155.

Grass, A. J. and Hosseinzadeh-Dalir, A. 1995 A simple theoretical model for estimating maximum scour depth under seabed pipelines. Paper No. 3D12. *Proceedings XXVI Congress of IAHR HYDRA 2000*, Vol. 3, pp. 281–286. London: Thomas Telford.

Grass, A. J., Raven, P. W. J., Stuart, R. J. & Bray, J. A. 1984 The influence of boundary layer velocity gradients and bed proximity on vortex shedding from free spanning pipelines. *ASME Journal of Energy Resources Technology* **106,** 70–78.

Kalghatgi, S. G. & Sayer, P. G. 1997 Hydrodynamics forces on piggyback pipeline configurations. *ASCE Journal of Waterway, Port, Coastal and Ocean Engineering Division* **123,** 16–22.

Kershenbaum, N. Y., Mebarkia, S. A. & Choi, H. S. 2000 Behavior of marine pipelines under seismic faults. *Ocean Engineering* **27,** 473–487.

Magda, W. 1997 Wave-induced uplift force acting on a submarine buried pipeline in a compressible seabed. *Computer and Geotechnics* **24,** 551–576.

Milne-Thomson, L. M. 1967. Theoretical Marine Hydrodynamics. 5th Ed. Hampshire: MacMillan Educated Ltd.

Müller, W. V. 1929 Systeme von Doppelquellen in der dbenen Strömung. *Zeitschrift für angewandte Mathematik und Mechanik* **9,** 200–213.

Neill, I. A. R. & Hinwood, J. B. 1998 Wave and wave-current loading on a bottom-mounted circular cylinder. *International Journal of Offshore and Polar Engineering* **8,** 122–129.

Nelder, J. A. & Mead, R. 1965 A simplex method for function minimization. *Computer Journal* **7,** 308–313.

Newman, J. 1978 *Marine Hydrodynamics*, 362–373. Cambridge, MA: The MIT Press.

Reddy, J. N. 1993 *An Introduction to the Finite Element Method*, 2nd edition. New York: McGraw-Hill.

Sabag, S. R., Edge, B. L. & Soedigdo, I. 2000 Wake II model for hydrodynamics forces on marine pipelines including waves and currents. *Ocean Engineering* **27,** 1295–1319.

Sarpkaya T. & Isaacson M. 1981 *Mechanics of Wave Forces on Offshore Structures*. New York: Van Nostrand Reinhold.

TAkahashi, T. & Bando, K. 1998 Hydrodynamics forces acting on arbitrary-shaped offshore structures subjected to seismic excitation. *Coastal Engineering Journal* **40,** 207–221.

Zdravkovich, M. M. 1985 Forces on a circular cylinder near a plane wall. *Applied Ocean Research* **7,** 197–201.

Zong, Z. & Lam, K. Y. 2000*a* Flexural response of a submarine pipeline to an underwater explosion bubble. *ASME Journal of Offshore Mechanics and Arctic Engineering* **122,** 194–199.

Zong, Z. & Lam, K. Y. 2000*b* Hydrodynamics influences on the ship hull vibration in shallow water. *Journal of Engineering Mathematics* **37,** 363–374.